

## Decreased melanoma CSF-1 secretion by Cannabigerol treatment reprograms regulatory myeloid cells and reduces tumor progression

Iris Wyrobnik<sup>a</sup>, Miryam Steinberg<sup>a</sup>, Anat Gelfand<sup>a</sup>, Ronen Rosenblum<sup>a</sup>, Yara Eid Mutlak<sup>a</sup>, Liron Sulimani<sup>b,c</sup>, Shiri Procaccia<sup>a</sup>, Yishai Ofran<sup>d</sup>, Hila Novak-Kotzer<sup>a</sup>, and David Meiri<sup>a</sup>

<sup>a</sup>The Laboratory of Cancer Biology and Cannabinoid Research, Department of Biology, Technion-Israel Institute of Technology, Haifa, Israel; <sup>b</sup>The Kleinfeld Laboratory, Department of Biology, Technion-Israel Institute of Technology, Haifa, Israel; <sup>c</sup>Cannasoul Analytics, Caesarea, Israel; <sup>d</sup>Department of Hematology, Shaare Zedek Medical Center and Faculty of Medicine, The Hebrew University of Jerusalem, Jerusalem, Israel

### ABSTRACT

During solid tumor progression, the tumor microenvironment (TME) evolves into a highly immunosuppressive milieu. Key players in the immunosuppressive environment are regulatory myeloid cells, including myeloid-derived suppressor cells (MDSCs) and tumor-associated macrophages (TAMs), which are recruited and activated via tumor-secreted cytokines such as colony-stimulating factor 1 (CSF-1). Therefore, the depletion of tumor-secreted cytokines is a leading anticancer strategy. Here, we found that CSF-1 secretion by melanoma cells is decreased following treatment with Cannabis extracts. Cannabigerol (CBG) was identified as the bioactive cannabinoid responsible for the effects. Conditioned media from cells treated with pure CBG or the high-CBG extract reduced the expansion and macrophage transition of the monocytic-MDSC subpopulation. Treated MO-MDSCs also expressed lower levels of iNOS, leading to restored CD8+ T-cell activation. Tumor-bearing mice treated with CBG presented reduced tumor progression, lower TAM frequencies and reduced TAM/M1 ratio. A combination of CBG and αPD-L1 was more effective in reducing tumor progression, enhancing survival and increasing the infiltration of activated cytotoxic T-cells than each treatment separately. We show a novel mechanism for CBG in modulating the TME and enhancing immune checkpoint blockade therapy, underlining its promising therapeutic potential for the treatment of a variety of tumors with elevated CSF-1 expression.

### ARTICLE HISTORY

Received 15 January 2023

Revised 24 May 2023

Accepted 24 May 2023

### KEYWORDS

Tumor Microenvironment; Regulatory Myeloid Cells; CSF-1 (M-CSF); MDSC; TAM; Cannabis; Cannabinoids; CBG; immune checkpoint inhibitors; αPD-L1

### Introduction

During solid tumor progression, the tumor microenvironment (TME) frequently evolves into a highly immunosuppressive milieu<sup>1,2</sup>. Key players in the formation of this anti-inflammatory environment are regulatory myeloid cells, such as tumor-promoting (M2-like) tumor-associated macrophages (TAMs) and myeloid-derived suppressor cells (MDSCs)<sup>2,3</sup>. Regulatory myeloid cells are recruited, polarized and activated by tumor-secreted cytokines and chemokines, such as colony-stimulating factor 1 (CSF-1, also known as M-CSF), monocyte chemoattractant protein-1 (MCP-1, also known as CCL2) and macrophage inflammatory protein-2 (MIP-2, also known as CXCL2)<sup>1,2</sup>. For example, CSF-1 is one of the cytokines that prevent MDSCs differentiation into mature myeloid cells<sup>4</sup> and under pathological conditions leads to the expression of the M2 transcriptome<sup>5</sup>. Additionally, blocking the CSF-1 receptor was shown to stop the accumulation of immunosuppressive TAMs<sup>6</sup>.

The generation and expansion of regulatory myeloid cells are one of the main mechanisms adopted by cancer cells to ensure tumor progression and metastasis formation<sup>7</sup>. For example, once activated, MDSCs express

various immunosuppressive markers, such as inducible nitric oxide synthase (iNOS) and Arginase-1 (Arg-1), leading to reduced CD8+ T-cell proliferation and activation<sup>8,9</sup>. This is one of the reasons why many patients fail to respond to immune checkpoint blockade therapies<sup>10</sup>. One promising strategy in targeting regulatory myeloid cells is the depletion of tumor-secreted cytokines to achieve a reduction in their expansion and activation<sup>11</sup>.

Medical Cannabis and its unique metabolites known as phytocannabinoids are gaining momentum in the field of drug development. They are intensely investigated for their potential anti-cancer functions and the effect of phytocannabinoids on the immune system has been described previously<sup>12,13</sup>. Phytocannabinoids modulate many processes in the body through their interaction with the endocannabinoid system, a ubiquitous and conserved neuromodulatory signaling system<sup>12,13</sup>. The endocannabinoid system is involved in the regulation and proper functioning of most physiological systems; thus, phytocannabinoids have a huge potential to influence a variety of physiological processes and exert therapeutic effects in different diseases<sup>14,15</sup>. The most commonly known phytocannabinoids, (–)-trans-Δ<sup>9</sup>-

**CONTACT** Hila Novak-Kotzer  [nhila@technion.ac.il](mailto:nhila@technion.ac.il); David Meiri  [dmeiri@technion.ac.il](mailto:dmeiri@technion.ac.il)  The Laboratory of Cancer Biology and Cannabinoid Research, Department of Biology, Technion-Israel Institute of Technology, Technion City Room 401, Haifa 3200003, Israel;

 Supplemental data for this article can be accessed online at <https://doi.org/10.1080/2162402X.2023.2219164>

© 2023 The Author(s). Published with license by Taylor & Francis Group, LLC.

This is an Open Access article distributed under the terms of the Creative Commons Attribution-NonCommercial License (<http://creativecommons.org/licenses/by-nc/4.0/>), which permits unrestricted non-commercial use, distribution, and reproduction in any medium, provided the original work is properly cited. The terms on which this article has been published allow the posting of the Accepted Manuscript in a repository by the author(s) or with their consent.

tetrahydrocannabinol (THC) and Cannabidiol (CBD), are extensively studied for therapeutic purposes<sup>14,16</sup>. However, very little is known about the other phytocannabinoids, although they were suggested to exert a variety of effects in pathological conditions<sup>17–20</sup>.

Most previous studies investigated the direct effect of medical Cannabis on cancer cells, without taking the complexity of the tumor ecosystem into consideration. A few studies focused on the effect of single cannabinoids, mostly THC or CBD, on MDSCs in healthy mice or immune-related diseases<sup>21,51</sup>. However, it is still not clear how whole Cannabis extracts or minor cannabinoids affect regulatory myeloid cell populations and what role these cannabinoids play in the TME.

In the current study, we aimed to investigate whether medical Cannabis can affect the cytokine secretion pattern of melanoma cells. Melanoma is one of the most immunogenic tumors and therefore it acquires different mechanisms to escape immune surveillance during tumor progression, one of which is the over-production of negative modulators of immune cells<sup>22</sup>. By altering the secretion of cytokines in the TME and thereby altering the characteristics of regulatory myeloid cells, immune evasion may be reduced and tumor progression may be halted. Here, we show a novel mechanism by which the single cannabinoid, Cannabigerol (CBG), modulates the differentiation and activation of regulatory myeloid cells leading to reduced cancer progression.

## Materials and methods

### Reagents

Synthetic CBG (Symrise, Germany, Cat# 664714) and synthetic Cannabinol (CBN; Open Book Extracts, Cat# IOB\_JACGA\_CBN) were diluted in DMSO (Merck Millipore, Cat#101900) to stock solutions.

### Cell lines and culture conditions

The murine melanoma cell line B16F10 was generously given to us as a gift from Dr. Yishai Ofran of Shaare Zedek Medical Center in Jerusalem. The human melanoma cell line A375 was purchased from ATCC (Cat# CRL-1619, RRID:CVCL\_0132). B16F10 cells were incubated in RPMI (Sigma, Cat# R8758) and A375 in DMEM (Sigma, Cat# D5796), supplemented with 10% FBS (Sigma, Cat# F7524) and 1% Penicillin/Streptavidin (Sartorius, Cat# 03–031-1B) at 37°C with 5% CO<sub>2</sub>.

### Apoptosis assay

Apoptosis was assessed by flow cytometry, measuring cells stained for Annexin V (BioLegend, Cat# 640941, 1:100) and propidium iodide (PI, BioLegend, Cat# 421301, 1:400) with indicated treatments. Stained cells were analyzed by BD FlowJo™ software version x.0.7 (BD Biosciences). Cell death was determined as the percentage of double positive cells.

### Cytokine screen

Conditioned media from treated B16F10 cells were collected, and cytokines and chemokines content were measured using the proteome profiler mouse cytokine array kit panel A (R&D Systems; Cat# ARY006) as described in the manufacturer's protocol.

### Elisa

The media from B16F10 and A375 cell lines, or homogenates from B16F10 tumors, were collected and the protein concentration of MCP-1, MIP-2, CCL5 and CSF-1 were measured by Quantikine Mouse M-CSF ELISA kit (R&D systems, Cat# MMC00) as described in the manufacturer's protocol.

### Immunofluorescence (IF) microscopy

B16F10 cells were treated with either synthetic CBG or Cannabis extract 3704 for 24 h. Then, cells were fixed with 4% PFA (Electron Microscopy Sciences, Cat# 15710) permeabilized, and blocked. Cells were then stained for CSF-1 (Santa Cruz; Clone D-4; Cat# 365779, RRID:AB\_10846852, 1:50), washed and stained with the secondary antibody anti-mouse Alexa Fluor 488-secondary antibody (Abcam, Cat# 150077, RRID:AB\_2630356, 1:500) and mounted with mounting solution containing DAPI (GBI labs, Cat# K1996619B). Samples were imaged using the Zeiss LSM 710 inverted confocal microscope with 20× (0.8NA) objective lens for statistical analysis and 63×/1.4 Oil objective lens for representative image acquisition. Analysis was conducted using the IMARIS software and results were calculated using the formula: mean AF-488 intensity divided by the number of nuclei.

### Mouse tumor model

To induce tumors, B16F10 cells were resuspended to a concentration of  $1 \times 10^6$  cells in 200  $\mu$ l sterile PBS and transplanted subcutaneously into the right flank of 8–10-week-old female WT C57BL/6 mice (Envigo Israel, 17.44 g  $\pm$  1.14 g) or male NOD-SCID IL2ry-null (NSG) mice (Technion animal facility, Israel). After either 24 h or 3 d, mice were randomly divided into groups and treated as indicated with either a vehicle of Cannabis extract solvent (18:1:1 ratio of DDW + 0.9% NaCl, Sigma, Cat# S7653; Cremophor® EL, Cat# 238470; Ethanol, Sigma, #Cat 111,727), CAN (100 mg/kg), synthetic CBG (2.5 mg/kg) or 3704 (3.75 mg/kg). Tumor volume was measured from day 10 to the endpoint (day 14–21) using a vernier caliper and calculated according to the formula  $(\text{length} \times \text{width}^2)^{0.5}$ . Treatment with isotype control (Bio X Cell, Cat# BP0090, 200  $\mu$ g/mouse) or  $\alpha$ -PD-L1 (Bio X Cell, Cat# BE0101, RRID:AB\_10949073, 200  $\mu$ g/mouse) commenced on day 3 and administrated every 4 d. For the survival analysis, mice bearing a tumor that had signs of ulcers or a volume higher than 1,000 mm<sup>3</sup> were euthanized.

To prepare single-cell suspensions from the tumors, on day 14 the tumors were excised from the mice and placed in Hanks' Balanced Salt solution (HBSS, Sigma; Cat# H6648) containing 20  $\mu$ g/ml DNase I (Sigma, Cat#

D5025), 1 mg/ml collagenase D from *Clostridium histolyticum* (Sigma-Aldrich, Cat# C5138) and 0.1 mg/ml hyaluronidase (Sigma-Aldrich, Cat# 6254). Tumors were mechanically digested using a scalpel and the gentleMACS™ Dissociator (Miltenyi Biotec). After centrifugation, the supernatant was further used for cytokine and chemokine concentration measurements. For the characterization of myeloid cell frequencies in tumors, cells were resuspended in 40% percoll gradient solution (prepared from 100% percoll, Cytiva, #17089101) and then 80% percoll was added on top of the 40% solution without mixing. Cells were isolated from the interphase between the 40% and 80% percoll solutions. Subpopulation frequency was measured by spectral flow cytometry using Cytex® Aurora (Cytex Biosciences), and cell count was measured by Countbright absolute counting beads (Cat# C36950, Invitrogen).

### ***In-vitro* Bone Marrow derived-MDSC differentiation (BM-MDSC)**

Bone-marrow-derived cells (BMDCs) were isolated from the fibula and tibia bones of healthy female WT C57BL/6 mice (8–12-week-old). Cells were counted, and  $1 \times 10^6$  cells were seeded in complete RPMI (Sigma, Cat# R8758) containing 10% FBS (Sigma, Cat# F7524), 1% L-Glutamine (Sartorius, Cat# 03-020-1B), 1% Penicillin/Streptavidin (Sartorius, Cat# 03-031-1B), 1% MEM-Eagle (Sartorius, Cat# 01-340-1B), 2.5% HEPES (Sartorius, Cat# 03-025-1B) and 1% sodium pyruvate (Sartorius, Cat# 03-042-1B) and supplemented with 20 ng/ml of GM-CSF and IL-6 (R&D systems, 415-ML and 406-ML). BMDCs were incubated for 4 d and then treated with conditioned media of treated B16F10 cells.

### ***BM-MDSCs CD8+ T-cell co-culture suppression assay***

Generated BM-MDSCs were treated with conditioned media for 24 h, then sorted into monocytic (MO)-MDSC and polymorphonuclear (PMN)-MDSC subsets. Concurrently, CD8+ T-cells were isolated from the spleens of healthy female WT C57BL/6 mice. To isolate CD8+ T-cells, spleens were mechanically disintegrated and the red blood cells were lysed with the red blood lysis buffer (Biological industries, Cat# 01-888-1B). CD8+ T-cells were isolated using the EasySep Mouse CD8+ T-cell isolation kit (Stemcell Technologies, Cat # 19853) according to the manufacturer's protocol.

Post-sorted MDSC subpopulations were co-cultured in complete RPMI with CD8+ T-cells that were activated with Dynabeads® (Cat# 11456D;  $12.5 \mu\text{l}/1 \times 10^6$  cells). After 48 h, the activation beads were removed and cells were incubated with eBioscience Cell Stimulation Cocktail (Invitrogen, Cat# 00-4970-93) for 3 h and then also with BD GolgiStop™ Protein Transport Inhibitor (BD Biosciences, Cat# 51-2092KZ). Intracellular staining of IFN- $\gamma$  and Granzyme B in CD8+ T-cells was achieved by using the BD Cytotfix/Cytoperm™ Kit (BD Biosciences, Cat# 554714) as stated in the manufacturer's instructions.

### ***Fluorescent activated cell sorting (FACS)***

To analyze the two subpopulations of BM-MDSCs, the cells were stained with Ly6C-BV421 and Ly6G-APC and sorted into MO-MDSC or PMN-MDSC using the BD FACSAria III Cell Sorter instrument (BD Biosciences). Directly after sorting, the two separate subpopulations were co-cultured with CD8+ T-cells or lysed and further analyzed via Western blot. A full list of antibodies used for flow cytometry assays can be found in the Supplemental materials.

### ***Preparation of cell lysates and Western Blot***

B16F10 cells, and sorted MO-MDSC and PMN-MDSC achieved as described, were lysed in RIPA buffer (Sigma, Cat# R0278) supplemented with Protease/Phosphatase Inhibitor Cocktail (Cell signaling, Cat# 5872S). Total protein concentrations were measured using the detergent-compatible protein assay (Bio-Rad, Cat# 5000113 and 5000114) and equal amounts were used. Primary antibodies used were CSF-1 (Santa Cruz; Clone D-4; Cat# sc -365779, RRID: AB\_10846852), iNOS (Abcam, Clone Cat# ab15323, RRID: AB\_301857) or GAPDH (Cell Signaling Technology, Clone 14C10, Cat# 3683S, RRID:AB\_1642205).

### ***Statistical analysis***

The data were analyzed by GraphPad Prism 6 (GraphPad Software Inc.), and the results were presented as mean  $\pm$  SEM. Comparisons were performed using one- or two-way ANOVA followed by post hoc Tukey's analysis or a student's t-test as indicated. A p-value  $<0.05$  was considered statistically significant.

### ***Study approval***

All procedures involving animals were conducted in accordance with the standards approved by the Technion Animal Care and Use Ethics Committee and the studies adhered to the Technion Code for Experimentation on Animals.

## **Results**

### ***CSF-1 secretion is reduced after treatment with a high-THC Cannabis extract***

We have previously shown that Cannabis extracts differ greatly in their phytocannabinoid profile<sup>23</sup> and therefore in their anticancer activity<sup>12</sup>. While some extracts exerted apoptotic effects, others influenced the dormancy state of cancer cells<sup>24</sup>. Regulatory myeloid cells were found to play key roles in promoting cancer dormancy and progression<sup>22</sup>. Therefore, in the current study, we focused on the effect of Cannabis and its bioactive metabolites, the phytocannabinoids, on the characteristics of myeloid cells in the TME. First, we chose a Cannabis extract (CAN) that we observed affects B16F10 tumor size *in-vivo* in wild-type (WT) mice (Figure 1a,b) but not in immunodeficient mice (Figure 1c). The major phytocannabinoids in this whole Cannabis extract were identified using Ultrahigh-performance

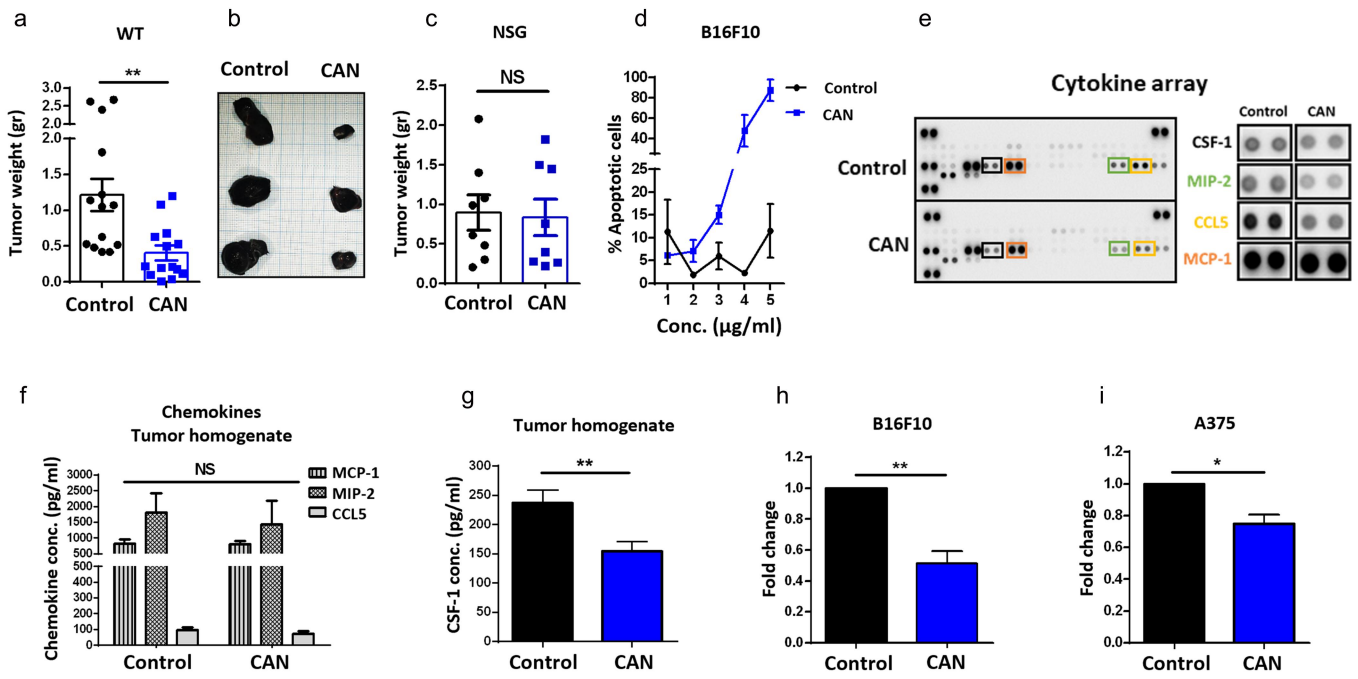


**Figure 1.** Cannabis extract treatment leads to a specific reduction in CSF-1 secretion by melanoma cells. (a) WT C57B6/L female mice (8–10-week-old,  $n=14$ ) were subcutaneously injected with  $1 \times 10^6$  B16F10 cells. After 24 h, mice were randomly divided into two groups and treated with either vehicle or the high-THC Cannabis chemovar CAN (100 mg/kg). After 14 d, the mice were sacrificed, and the tumors were excised and weighed. (b) Representative image of excised tumors from mice treated with vehicle (left) or CAN (right). (c) Immunodeficient NSG male mice (8-week-old,  $n=8$ ) were treated as in a. After 14–15 d, the tumors were excised and weighed. (d) B16F10 cells were treated with a control (DMSO) or increasing concentrations of CAN extract for 24 h ( $n=1-4$ ). Cell death was evaluated by APC Annexin V/PI staining and apoptotic cells were measured using flow cytometry. (e) B16F10 cells were treated with 2 µg/ml of CAN and assessed for cytokine secretion with the proteome profiler cytokine array. Representative membranes of the cytokine screen are depicted and four selected cytokines: CSF-1, MIP-2, CCL-5 and MCP-1 are shown in higher magnification. (f-g) The concentrations (pg/ml) of MCP-1, MIP-2, CCL5 and CSF-1 were measured using ELISA in tumor homogenates that originated from B16F10 tumors of mice treated over a period of 2 weeks with either Cannabis extract solvent (Control) or CAN ( $n=5-23$ /group). (h-i) Change in secreted CSF-1 concentration in the supernatants of B16F10 cells treated with 2 µg/ml (h) and A375 (i) treated with 6 µg/ml of CAN ( $n=4-6$ ). Results were normalized to control group, presented as average  $\pm$  SEM and statistically analyzed by a student's *t*-test (NS – non-significant, \* $p < 0.05$ , \*\* $p < 0.01$ ).

liquid chromatography with an ultraviolet detector (HPLC/UV) according to the retention time of each specific phytocannabinoid and were found to contain mainly THC (66%) and other phytocannabinoids in lower percentages (0.08%–1.66%) (Supplemental STable 1, Supplemental materials). When the B16F10 cell line was treated with CAN, we decided to focus on a concentration that affects the cells without inducing cell death, so that we could assess differences in cytokine secretion. The cells were treated with increasing concentrations of CAN, and we identified 2 µg/ml as the optimal concentration which does not lead to increased cell death (Figure 1d). Using a cytokine screen array, a reduction in three myeloid-related cytokines and chemokines was detected, namely CSF-1, MIP-2 and C-C Motif Chemokine Ligand 5 (CCL5) (Figure 1e). Changes in MCP-1 secretion were not detected; however, MCP-1 concentrations were tested in further experiments as a positive control (Figure 1e). To validate the change in secretion observed by the B16F10 cell line, the four above indicated cytokines and chemokines were measured in B16F10 tumors from mice that were treated either with a control vehicle or with CAN using an enzyme-linked immunosorbent assay (ELISA). We were able to detect only a reduction in the concentration of CSF-1 in tumors of CAN-treated mice (Figure 1f,g). *In-vitro* validation of CSF-1 secretion by B16F10 cell line and the human A375 melanoma cells showed the reduced secretion of CSF-1 by CAN-treated cells as well (Figure 1h-i). The optimal concentration of CAN for

A375 was assessed in a similar manner to B16F10 and found as 6 µg/ml *in-vitro* (Supplemental Figure 1a, leftmost columns).

### CBG reduces CSF-1 secretion by B16F10 cells

Since we identified the specific reduction of CSF-1 after CAN treatment, we continued investigating the specific phytocannabinoids present in the whole extract that are responsible for the seen effects. For this purpose, CAN extract was fractionated into four fractions F1-F4 (Figure 2a, Supplemental materials). The major phytocannabinoids in each fraction are shown in Supplemental STable 1. Then, B16F10 cells were treated with each fraction separately and all the possible combinations. The concentration of each fraction was normalized according to the concentration of the phytocannabinoid with the highest weight-to-weight percentage in the whole extract. We found that a combination of fractions F1 and F2 mimics the effect of the whole extract (Figure 2b). The phytocannabinoids with the highest weight-to-weight percentage in F1 were CBN and CBG. In F2, the major phytocannabinoid detected was THC and this fraction was almost exclusively composed of THC (93%). This led us to investigate the change in CSF-1 secretion on a single-molecule resolution. Synthetic pure CBN and synthetic pure CBG were tested in combination with F2, used as indicative of pure THC. We used the same concentrations of the cannabinoids as they are present in the whole extract, cells were treated separately or by any other cannabinoid combination

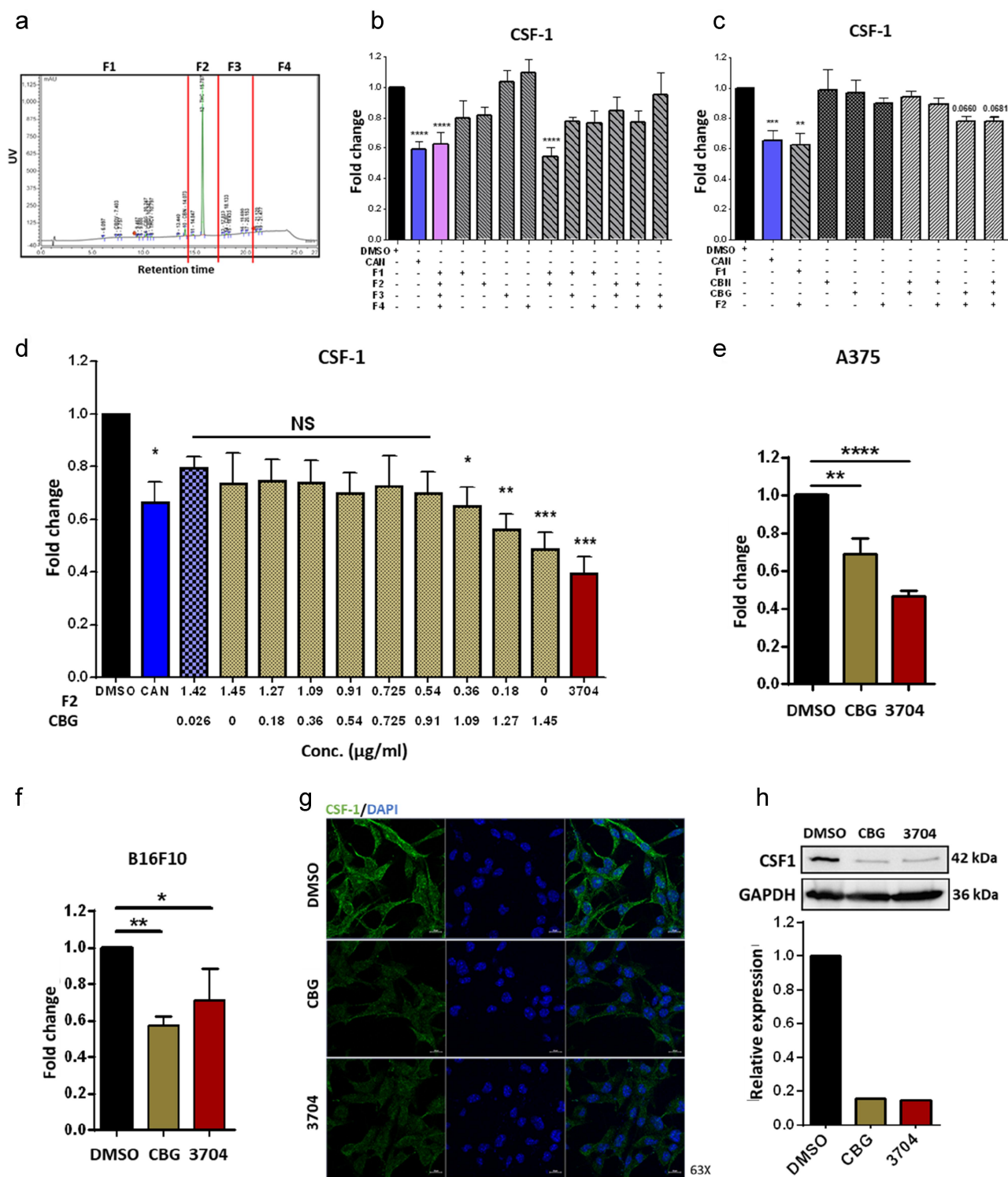


**Figure 2.** CBG reduces CSF-1 secretion by B16F10 cells. (a) Diagram of CAN chromatographic separation achieved using preparative HPLC/UV. CAN was separated into four fractions (F1-F4) according to their retention time using preparative HPLC/UV with a HALO C18 Fused-Core column and a ternary A/B/C multistep hydrophobic gradient. (b-d) CSF-1 secretion was measured by ELISA and normalized to DMSO control after treatment of B16F10 cells with (b) CAN and different combinations of fractions F1-F4 from CAN extract, (c) CAN and different combinations of fractions F1-F2 and the synthetic cannabinoids in their concentrations as in the whole extract, CBN (0.04  $\mu\text{g/ml}$ ) and CBG (0.026  $\mu\text{g/ml}$ ); and (d) different ratios of CBG and F2. (e) A375 cells were treated with 1.5  $\mu\text{g/ml}$  CBG and 2  $\mu\text{g/ml}$  3704 and CSF-1 secretion was measured using ELISA. Results were normalized to DMSO. (f) CSF-1 protein expression in B16F10 cells treated with either DMSO control, 1.5  $\mu\text{g/ml}$  CBG or 2  $\mu\text{g/ml}$  3704 was visualized by confocal microscopy using a 63X objective. The nuclei were visualized with DAPI. Relative AF-488 intensity of each treatment was normalized to the DMSO treatment. Each biological repeat included three random images taken,  $n=3$ . (g) Representative images of f. (h) B16F10 cells were treated as in e, then harvested with RIPA and the cell lysates were assessed for CSF-1 protein levels via Western blotting with anti-CSF-1 and GAPDH as the loading control. Results are shown as fold-change + SEM, and statistical significance was calculated with one-way ANOVA (NS – non-significant, \* $p < 0.05$ , \*\* $p < 0.005$ , \*\*\* $p < 0.0005$ , \*\*\*\* $p < 0.0001$ ).

(Figure 2c). The addition of synthetic CBN together with CBG and F2 did not further reduce CSF-1 secretion. However, the combination of CBG and F2 was not as efficient as the whole extract or F1 and F2 combined. Therefore, we tested the effect on CSF-1 secretion by different ratios of CBG and F2 (Figure 2d). Strikingly, with increasing concentrations of CBG up to 1.45 µg/ml and decreasing concentrations of F2, CSF-1 secretion was reduced more efficiently. As a positive control, we used a high-CBG chemovar, termed 3704, at the same concentration of 2 µg/ml as was used for CAN. We identified a more significant reduction in CSF-1 secretion compared to the original CAN extract (Figure 2d, *rightmost column*). These results were verified in the A375 cell line, cells treated with 1.5 µg/ml CBG and 2 µg/ml 3704 showed reduced CSF-1 secretion in this cell line as well (Figure 2e). Further validation was conducted by measuring CSF-1 protein levels in B16F10 cells treated with either 1.5 µg/ml CBG or 2 µg/ml 3704 using confocal microscopy or a Western blot assay (Figure 2f-h). The toxicity of all the different treatments at the indicated concentrations was measured, and no increased cell death was identified compared to DMSO (Supplemental Figure 1a-b).

### Conditioned media from CBG-treated B16F10 cells reduces MO-MDSC expansion and macrophage transition

Since CSF-1 is a key regulator of differentiation and expansion of the monocyte-macrophage axis<sup>4</sup>, we investigated how the reduction in CSF-1 secretion by CBG-treated B16F10 might influence the myeloid subpopulation frequency distribution *ex-vivo*. For this purpose, BM-MDSCs were treated as indicated in Figure 3a, myeloid frequencies were measured using flow cytometry after 24 h or 48 h and the gating strategy is shown in Figure 3b. As a control, we treated BM-MDSCs with control growth media with the same concentrations of DMSO, CBG and 3704 treatments as were added to the B16F10 cells. We found that the overall percentage of monocytes (Ly6C<sup>+</sup>/Ly6G<sup>-</sup> cells<sup>25</sup>) did not change when BM-MDSCs were treated with the different B16F10 CM nor with control growth media (Figure 3c). However, we identified a significant increase in the frequency of the Ly6C<sup>high</sup>/Ly6G<sup>-</sup> MO-MDSC subpopulation<sup>25</sup>, when BM-MDSCs were treated with CM from B16F10 (Figure 3d). Moreover, when BM-MDSCs were treated with CM from B16F10 treated with either CBG or 3704, we detected a significant decrease in MO-MDSC percentages compared to B16F10 treated with DMSO (Figure 3d). The effect was specific to the MO-MDSCs as PMN-MDSC frequencies (Ly6C<sup>+</sup>/Ly6G<sup>+25</sup>) were not affected by any treatment (Figure 3e).

During tumor progression, tumor-secreted CSF-1 mediates the differentiation of monocytes and MO-MDSC into anti-inflammatory macrophages<sup>11</sup>. Therefore, we investigated whether reduced CSF-1 secretion by CBG-treated B16F10 cells affects the transition of MO-MDSCs to alternatively activated F4/80<sup>+</sup> macrophages. We measured the expression of Arg-1 in the double-positive F4/80<sup>+</sup> and Ly6C<sup>+</sup> cells and ensured that the immunosuppressive phenotype in those cells is conserved when they were treated with B16F10 CM for 48 h (Supplemental Figure 2a). We identified a reduction of F4/80 expression by Ly6C<sup>+</sup> cells when CM from B16F10 cells treated with CBG or 3704 was added compared to DMSO. This trend

was apparent after 24 h (Figure 3f) and was statistically significant after 48 h (Figure 3g).

### Treated MO-MDSCs express lower levels of iNOS leading to restored CD8+ T-cell activation

Our results showed that reduced CSF-1 secretion by B16F10 cells treated with CBG or 3704 specifically affects the expansion of Ly6C<sup>high</sup> MO-MDSC and reduces the transition to F4/80 expressing macrophages *ex-vivo*. We hypothesized that the reduced MO-MDSC expansion is associated with decreased immunosuppressive properties as well. To test this, BM-MDSCs were generated and treated as mentioned above. After 24 h, the expression of the immunosuppressive markers Arg-1 and iNOS<sup>8,9</sup> by the BM-MDSC subpopulations was assessed using flow cytometry. Arg-1 expression in MO-MDSCs and PMN-MDSCs did not change significantly when cells were treated with CM from B16F10 cells compared to when cells were treated with control growth media (Supplemental Figure 2b,c). In addition, when BM-MDSCs were exposed to CM of CBG- or 3704-treated B16F10, no significant difference was detected in Arg-1 expression compared to CM of DMSO-treated B16F10 cells in neither of the MDSC subpopulations (Supplemental Figure 2c,b). However, the expression of iNOS by BM-MDSCs increased significantly for the subset of MO-MDSCs when the CM of DMSO-treated B16F10 cells was added to the BM-MDSCs (Figure 4a, *gray*). The addition of CM of CBG- or 3704-treated B16F10 cells significantly decreased iNOS expression in specifically MO-MDSC compared to CM of DMSO treated B16F10 cells (Figure 4a, *yellow, red*). iNOS expression also increased by PMN-MDSCs when CM of DMSO-treated B16F10 cells was added (Figure 4b, *gray*), although not to the same extent as the MO-MDSC subset. Additionally, no significant decrease in iNOS expression by PMN-MDSC was detected, when exposed to CM of CBG- or 3704-treated B16F10 cells compared to CM of DMSO-treated B16F10 cells (Figure 4b). To exclude the possibility of direct effects of CBG and 3704 on iNOS expression by MDSCs, BM-MDSCs were generated as described and added medium from untreated B16F10 to the cells together with either DMSO, CBG or 3704. iNOS expression was measured in each subpopulation and no significant differences were detected (Supplemental Figure 3a,b), indicating that the observed effect is mediated through the change in tumor cytokine secretion in the TME.

For further validation, BM-MDSCs were generated and sorted into MO-MDSC and PMN-MDSC subsets; then, iNOS expression was measured in each subpopulation by Western blot (Figure 4c). A reduction of iNOS expression was observed specifically in MO-MDSCs when CM from CBG- or 3704-treated B16F10 cells were added to the BM-MDSCs compared to CM of DMSO-treated B16F10 cells. Here again, PMN-MDSC expressed very low levels of iNOS.

Many studies have shown the involvement of increased iNOS expression by MDSCs in suppressing CD8+ T-cell activation in the TME<sup>8</sup>. Therefore, we tested the ability of sorted and treated BM-MDSC subpopulations to restore CD8+ activation *ex-vivo*. For this purpose, we established a co-culture experiment of CD8+ T-cells and MO-MDSCs or PMN-

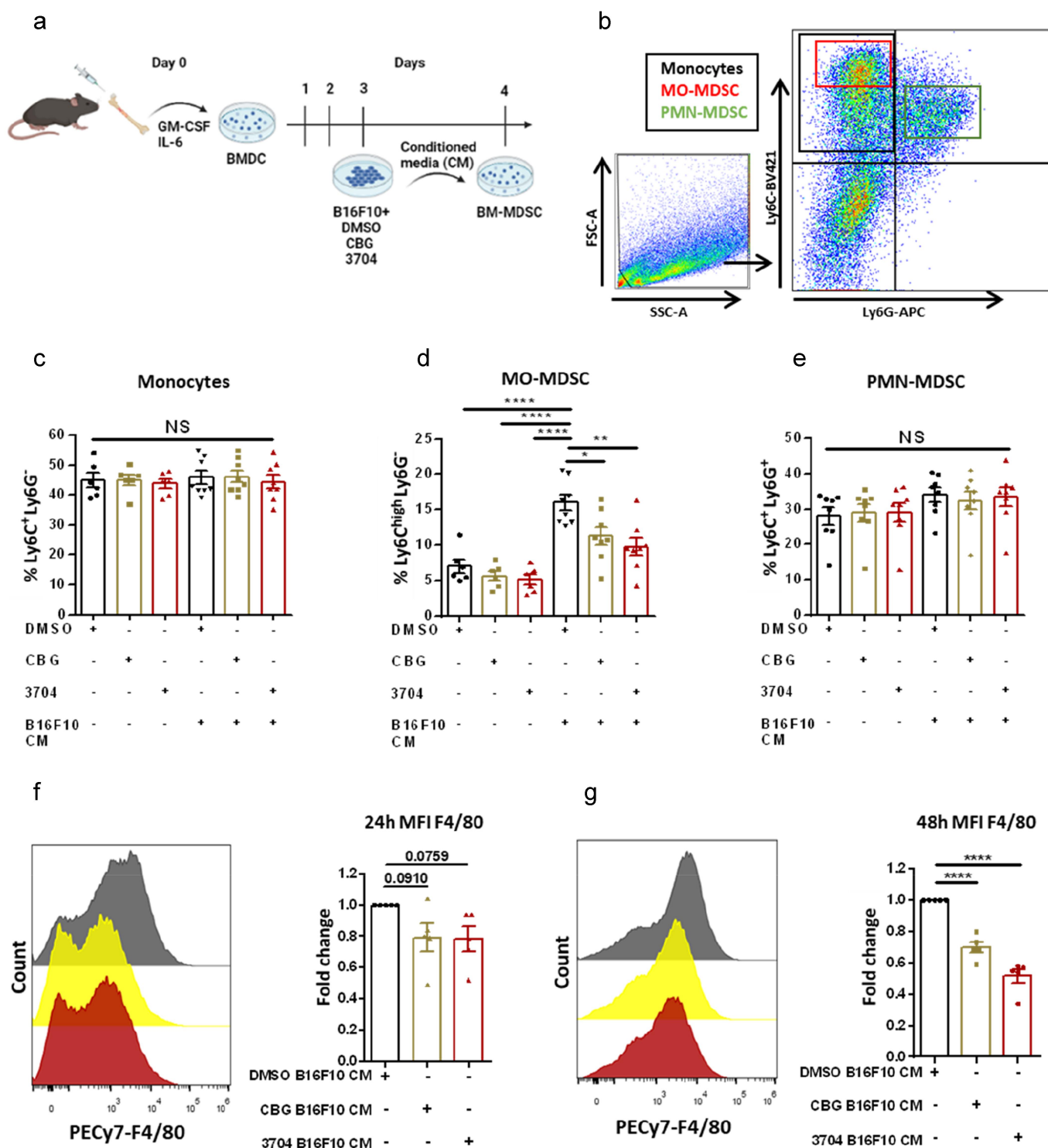


**Figure 3.** CM from CBG-treated B16F10 cells reduces MO-MDSC expansion and monocyte to macrophage transition. (a) Experimental design of *ex-vivo* generation of BM-MDSCs from WT C57BL/6 mice. BMDCs were supplemented with 20 ng/ml of GM-CSF and IL-6 (4 d) to induce MDSC differentiation. Concurrently, B16F10 cells were treated with either DMSO, CBG (1.5  $\mu$ g/ml) or the high-CBG extract 3704 (2  $\mu$ g/ml) for 24 h and the resulting conditioned media (CM) was used to treat the generated MDSCs. (b) FACS gating strategy of monocytes, MO-MDSC and PMN-MDSC (black, red and green rectangles, respectively). (c-e) The myeloid subpopulation frequencies of (c) monocytes, (d) MO-MDSCs and (e) PMN-MDSCs were measured using flow cytometry after treatment for 24 h of control growth media (no cells) with either DMSO, CBG or 3704 or CM from DMSO, CBG or 3704 treated B16F10 cells ( $n=6$ ). (f-g) Summary of the mean fluorescent intensity (MFI) of macrophage marker F4/80 of Ly6C<sup>+</sup> cells after 24 and 48 h, respectively, with the indicated treatments ( $n=4$ ). A representative histogram is shown on the left. Results are shown as average or fold-change  $\pm$ SEM and statistical significance was calculated by one-way ANOVA (NS – non-significant, \* $p < 0.05$ , \*\* $p < 0.01$ , \*\*\*\* $p < 0.0001$ ).

MDSCs. After 48 h of co-incubation, CD8<sup>+</sup> T-cells were assessed for intracellular expression of Granzyme B (GrzB) and Interferon- $\gamma$  (IFN- $\gamma$ ) using flow cytometry (Figure 4d-g). GrzB expression levels were lowered in T-cells co-cultured

with MO-MDSCs exposed to the CM of DMSO-treated B16F10 cells (Supplemental Figure 4a). Moreover, a trend of restored GrzB expression was detected when T-cells were co-cultured with MO-MDSCs exposed to CM of CBG- or 3704-

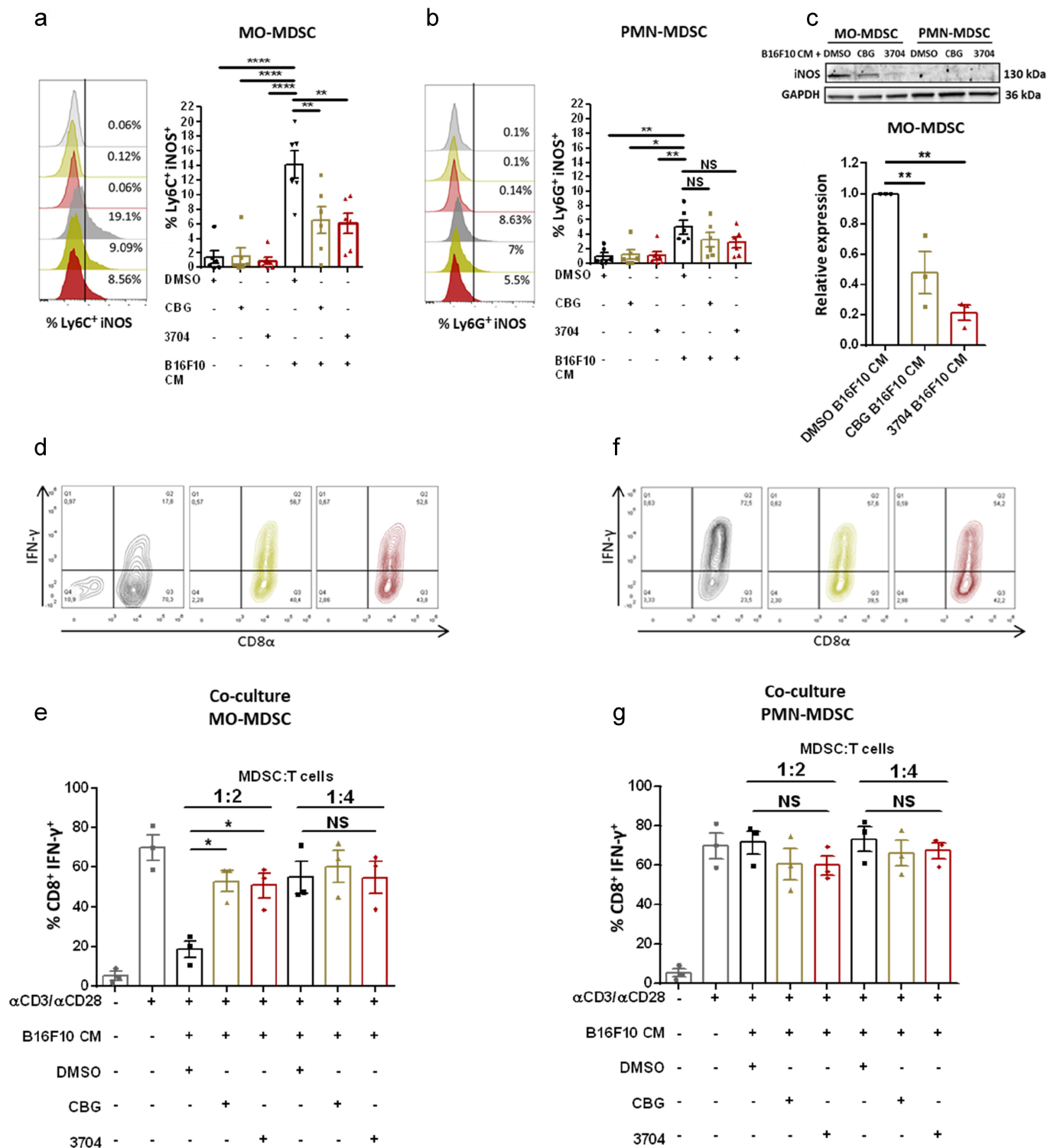


**Figure 4.** MO-MDSCs show reduced iNOS expression leading to restored IFN $\gamma$  expression by CD8 $^{+}$  T-cells when treated with CM from CBG- or 3704-treated B16F10 cells. (a-b) Percent of iNOS expression ( $n=6$ ) by MO-MDSCs (a) and PMN-MDSCs (b), representative flow charts are shown on the *left*. (c) BM-MDSC was sorted 24 h posttreatment into MO-MDSC and PMN-MDSC subpopulations. iNOS expression was measured by Western blotting with iNOS antibody and GAPDH as the loading control for each subpopulation separately. Representative blots are presented on the *top*, and the relative intensity of three independent repeats is presented on the *bottom*. Results are presented as relative expression compared to MO-MDSCs treated with CM from DMSO-treated B16F10 cells. (d-g) Generated BM-MDSCs were treated with conditioned media for 24 h, then sorted into MO-MDSC and PMN-MDSC subsets. The sorted MDSC subpopulations were co-cultured with activated CD8 $^{+}$  T-cells for 48 h. Then, CD8 $^{+}$  T-cells were prepared for intracellular staining and stained with IFN- $\gamma$ -FITC. The frequencies of CD8 $^{+}$  IFN- $\gamma$  $^{+}$  cells were measured with flow cytometry and are presented with the matching contour plots for co-culture with MO-MDSCs (d-e) and PMN-MDSCs (f-g). Graphs are shown as average  $\pm$  SEM and statistically analyzed by one-way ANOVA (NS – non-significant, \* $p < 0.05$ , \*\* $p < 0.01$ , \*\*\*\* $p < 0.0001$ ).

treated B16F10 cells (Supplemental Figure 4a). The co-culture of T-cells with PMN-MDSCs exposed to CM of DMSO-treated B16F10 cells did not result in reduced GrzB expression (Supplemental Figure 4b, *gray*) and a trend of reduced GrzB expression was detected when T-cells were co-cultured with PMN-MDSC exposed to CM of CBG- or 3704-treated B16F10 cells (Supplemental Figure 4b). We found that MO-MDSCs specifically exposed to CM of DMSO-treated B16F10 cells suppressed significantly CD8+ T-cell IFN- $\gamma$  expression compared to PMN-MDSCs that received the same treatment (Figure 4d-g). Additionally, when CM of CBG- or 3704-treated B16F10 was added to MO-MDSCs, a restoration of CD8+ IFN- $\gamma$  expression was observed in a dose-dependent manner (Figure 4e). In contrast, CD8+ T-cells co-cultured with PMN-MDSCs showed no significant changes with either of the treatments (Figure 4g).

### **CBG treatment reduces B16F10 tumor progression and TAM frequencies in the tumors**

As the next step, we measured B16F10 tumor development in WT mice that were treated with CBG or 3704 and investigated the frequencies of the myeloid cell subpopulations in the tumors. Tumor weight and tumor volume were significantly lower in the CBG-treated group compared to the vehicle-treated group and a similar trend of smaller tumor weight and volume was evident in the 3704-treated group (Figure 5a-c). To confirm the presence of CBG in the tumors, we analyzed its concentration in all tumors by liquid Chromatography with tandem mass spectrometry (LC-MS/MS)<sup>18</sup> and found it is present in the treated groups, but not in the control group (Figure 5d). As CBG treatment was the most effective in reducing tumor progression, we focused on investigating myeloid subpopulations in this group. To assess the subpopulations of myeloid cells in the spleens and tumors, single-cell suspensions were prepared from both organs and stained with specific extracellular markers (Figure 5e-k; Supplemental Figure 5b,c). CBG-treated mice had reduced MO-MDSC frequencies in the spleen; however, no change was detected in the tumor (Figure 5e,f). Treatments did not affect the frequencies of the PMN-MDSC subpopulation in the spleen or the tumor (Figure 5g,h), further indicating the specificity of CBG treatment to CSF-1 secretion and by that to the MO-MDSC subpopulation. As continuous CSF-1 secretion by tumor cells into the TME shifts the M1/TAM ratio in favor of the TAMs<sup>5</sup>, we tested macrophage subpopulation frequencies in the tumor. There was a strong trend of a decreased frequency in TAMs in the CBG-treated group relative to vehicle control (Figure 5j). Further, we analyzed the ratio between the pro-inflammatory M1 macrophages<sup>25</sup> and the anti-inflammatory TAMs and found a significant difference of decreased ratio in the CBG-treated group relative to vehicle control, indicative of a reduced shift of pro-inflammatory macrophages toward TAMs and a less immunosuppressive TME (Figure 5k).

### **A combination of CBG and $\alpha$ PD-L1 is more effective than each treatment separately**

A common immune checkpoint blockade therapy in melanoma is anti-programmed cell death ligand 1 ( $\alpha$ PD-L1)<sup>26</sup>. Recent studies revealed that in many cases it is insufficient to use such therapy alone<sup>27,28</sup> as the presence of immunosuppressive myeloid cells reduces its efficacy<sup>26,29</sup>. Hence, as CBG treatment shifted the TME into a less immunosuppressive milieu, we tested whether a combination of CBG with  $\alpha$ PD-L1 can improve its anticancer effects. Mice were treated with either a control or CBG and concurrently administered  $\alpha$ PD-L1 (Figure 6a). The activity of intra-tumoral MO-MDSCs was assessed according to iNOS expression levels (Figure 6b-d). A trend of reduction in iNOS expression was detected in both treatment groups, indicating that these cells are less immunosuppressive in both the treatment groups, the CBG and CBG together with  $\alpha$ PD-L1. Further, tumor progression was analyzed by measuring tumor volume from day 10 to day 14 (Figure 6e). Separate treatment with either CBG or  $\alpha$ PD-L1 resulted in significantly reduced tumor volumes to a similar extent, approximately 60%-70%. Furthermore, co-treatment with CBG and  $\alpha$ PD-L1 led to a significant reduction in tumor volume relative to  $\alpha$ PD-L1 by itself and to the control group (Figure 6e,f). All mice in treatment groups had increased overall survival relative to the control, with the combined treatment significantly so. Further, intra-tumoral CD8+ T-cells were stained for GrzB and TNF- $\alpha$ . Leukocyte count per tumor weight was significantly higher in the co-treatment group, and a similar trend was evident in each of the separate treatment groups, indicating a higher infiltration of immune cells to the tumor (Figure 6h). For the cytotoxic T-cells, there was a trend of increased infiltration and activity by all treatments, and this trend was strongest in the co-treatment group (Figure 6i-k).

## **Discussion**

The therapeutic strategy of TME modulation is gaining attention in the field of anticancer treatment. Immune checkpoint blockade therapy has been in use for oncology patients over the last decade, alone or in combination<sup>30</sup>. Inhibitory antibodies such as  $\alpha$ PD-L1 disrupt the negative regulation between cancer cells and T-cells to harness the cytotoxic abilities of the immune system<sup>6</sup>. However, there are several molecular mechanisms allowing resistance to blockade therapy<sup>29</sup>. Recent studies revealed that it is insufficient to stimulate the cytotoxic T-cells with immune checkpoint blockade therapy, rather, concurrently targeting immunosuppressive cells<sup>8,29</sup>. We therefore set out to examine whether Cannabis extracts can immunomodulate the regulatory myeloid cells in the TME and enhance the existing immune-checkpoint blockade therapies.

Many clinical trials attempted modulating immunosuppressive cells by targeted depletion of tumor-secreted cytokines<sup>31,32,33</sup>, and as CSF-1 is a major modulator of regulatory myeloid cells in the TME, targeting the CSF-1 axis has been under extensive investigation. CSF-1 is highly expressed by several tumor types<sup>32,33</sup> and is associated with poor prognosis and survival<sup>32-35</sup>; emphasizing the relevance of targeting this cytokine. Moreover, CSF-1 is specific to the monocyte-macrophage axis, therefore its depletion does not

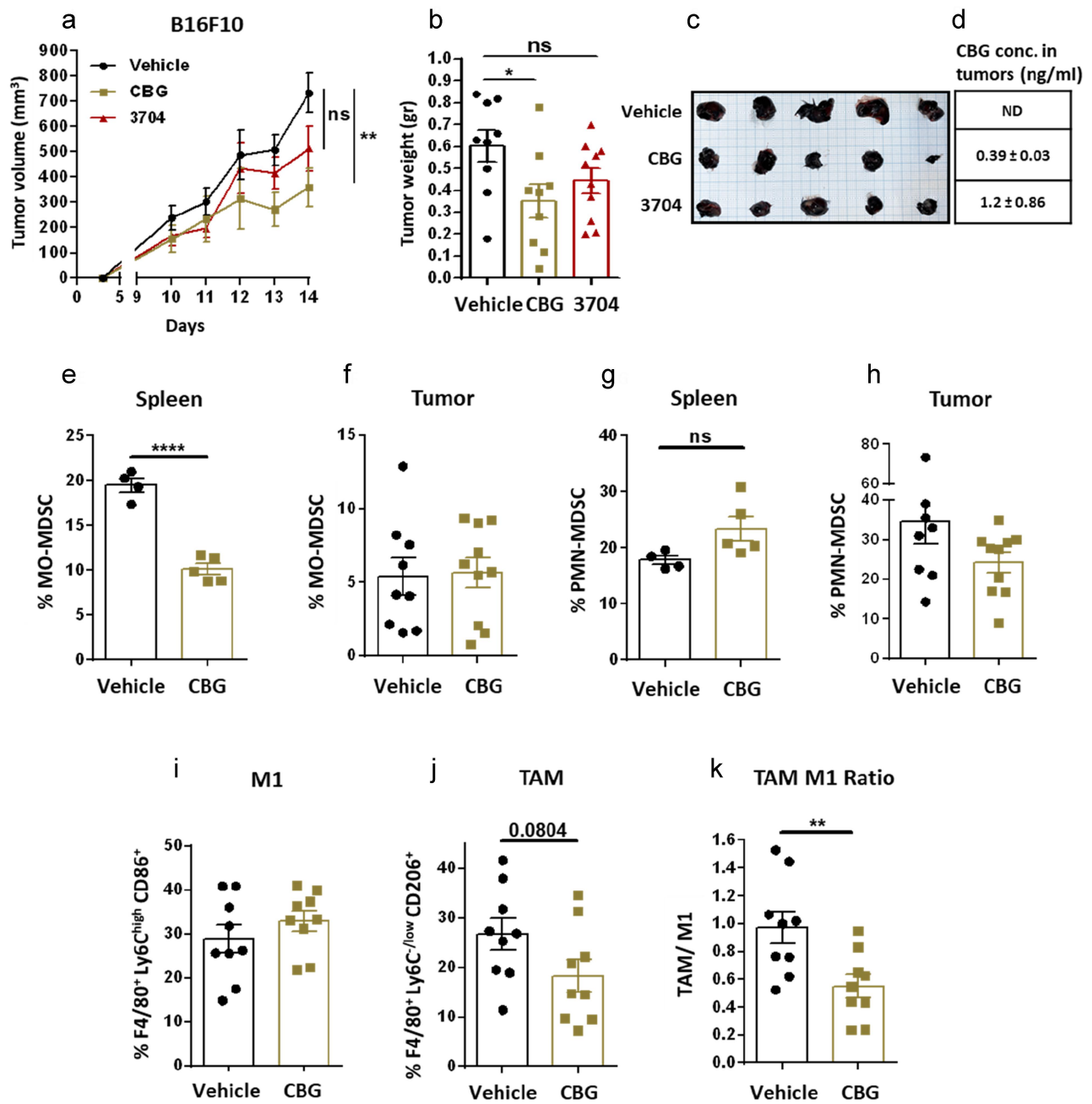


**Figure 5.** Synthetic CBG or high-CBG extract treatments reduce tumor progression and TAM macrophage frequencies in tumors. Female WT C57BL/6 mice ( $n=9-10$ /group, two independent experiments) were injected with  $1 \times 10^6$  B16F10 cells. After 3 d, the mice were treated intraperitoneally with either vehicle, synthetic CBG (2.5 mg/kg), or the high-CBG extract 3704 (3.75 mg/kg), as indicated, over the course of 14 d. (a) Growth curve of ectopic tumor volume in mice. Tumors were measured using a vernier caliper, and their volume was calculated according to the formula  $(\text{length} \times \text{width}^2) \times 0.5$ . (b) Averaged tumor weight (grams) per treatment group on day 14. (c) Image of excised tumors. (d) The concentration of CBG in tumor homogenates was evaluated with LC-MS/MS ( $n=4-5$ /group) and shown as mean  $\pm$  standard deviation (ND – not detected). (e-f) Single-cell suspensions were prepared from the excised spleens ( $n=4-5$ ) and tumors ( $n=9-10$ ), myeloid cell frequencies in the spleens were measured from total CD11b<sup>+</sup> cells and in the tumors from total CD45<sup>+</sup> cells. Extracellular markers for (e) CD11b<sup>+</sup> Ly6C<sup>high</sup> Ly6G<sup>-</sup> (f) CD45<sup>+</sup> F4/80<sup>-</sup> Ly6C<sup>high</sup> Ly6G<sup>-</sup> (g) CD11b<sup>+</sup> Ly6C<sup>low</sup> Ly6G<sup>+</sup> (h) CD45<sup>+</sup> F4/80<sup>-</sup> Ly6G<sup>+</sup> Ly6C<sup>low</sup> (i) CD45<sup>+</sup> F4/80<sup>+</sup> Ly6C<sup>high</sup> CD86<sup>+</sup> (j) CD45<sup>+</sup> F4/80<sup>+</sup> Ly6C<sup>low</sup> CD206<sup>+</sup> were used, and the frequencies were measured by spectral flow cytometry. (k) TAM/M1 frequency was calculated for each mouse, and the average ratio is presented for the indicated groups ( $n=9$ ). Statistically analyzed by one-way ANOVA (NS – non-significant, \* $p < 0.05$ , \*\* $p < 0.01$ ) for tumor volume and weight on day 14, and by a student t-test (\*\* $p < 0.01$ , \*\*\*\* $p < 0.0001$ ).

affect other immune cell populations, possibly making it more tolerable<sup>11</sup>. Our findings provide a new tool for targeting this major tumor-secreted cytokine with highly relevant clinical applications.

We succeeded to purify and identify from the whole extract a single cannabinoid, CBG, able to reduce CSF-1 secretion more efficiently than the psychoactive THC.

CBG is a non-psychoactive cannabinoid, which makes it more suitable for medical applications. Only a few studies investigated the pharmacological effects of CBG<sup>36</sup> and none tested its effects on the TME. To verify our findings for CBG, we utilized a high-CBG chemovar termed 3704 and found it was as efficient as pure CBG and more efficient than the high-THC chemovar in reducing CSF-1

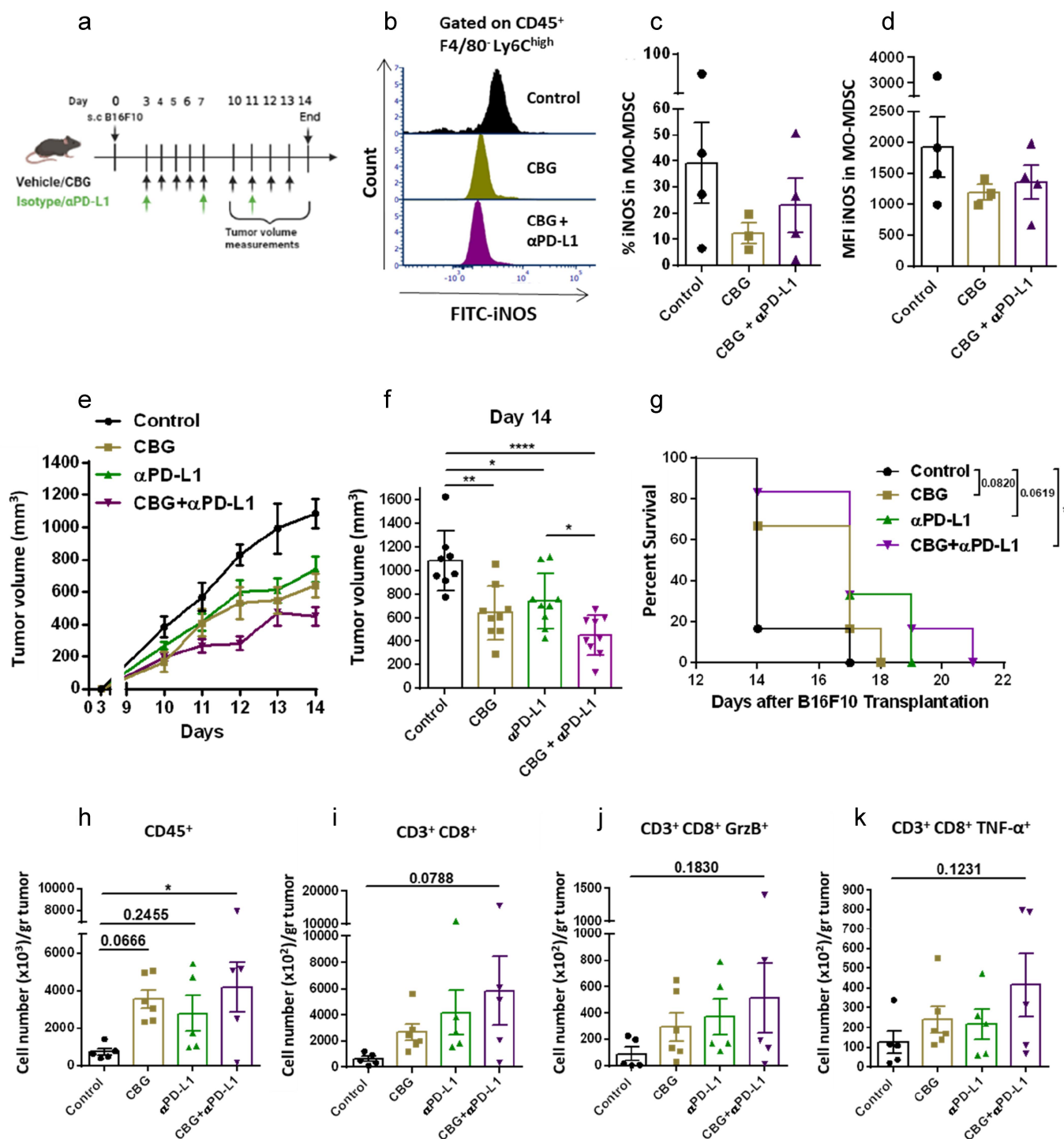


**Figure 6.** A combination of CBG and αPD-L1 is more effective than each treatment separately. (a) Diagram of the mice model experiment. Female WT C57BL/6 mice ( $n=5$ /group) were injected with  $1 \times 10^6$  B16F10 cells. After 3 d, the mice were divided randomly into groups and treated intraperitoneally with either vehicle and isotype control, synthetic CBG (2.5 mg/kg), αPD-L1 (200 μg/injection) or a combination of CBG and αPD-L1, over the course of 14 d, as indicated. (b-d) Single-cell suspensions were prepared from the excised tumors ( $n=3-4$ ), and MO-MDSCs were stained with the subpopulation of extracellular markers and additionally stained with the intracellular marker iNOS. (b) Representative flow charts of iNOS expression in CD45<sup>+</sup> F4/80<sup>+</sup> Ly6C<sup>high</sup> MO-MDSCs. iNOS percentage (c) and MFI (d) were analyzed by spectral flow cytometry. (e) Growth curve of ectopic tumor volume in mice. Tumors were measured using a vernier caliper, and their volume was calculated according to the formula (length  $\times$  width<sup>2</sup>)  $\times$  0.5. (f) Differences in tumor volume between groups were analyzed on day 14 and presented as mean  $\pm$  SEM of two independent experiments and plotted for percentiles 10–90 ( $n=8-9$ ). (g) Survival analyses after subcutaneous tumor transplantation ( $n=6$ ), statistical differences were calculated with the log-rank test ( $*p < 0.05$ ). (h-k) Immune cell number was normalized to the weight of each respective tumor, calculated using counting beads for (h) CD45<sup>+</sup> (i) CD45<sup>+</sup> CD3<sup>+</sup> CD8<sup>+</sup> (j) CD45<sup>+</sup> CD3<sup>+</sup> CD8<sup>+</sup> GrzB<sup>+</sup> and (k) CD45<sup>+</sup> CD3<sup>+</sup> CD8<sup>+</sup> TNF-α<sup>+</sup>. Statistical significance was calculated using one-way ANOVA ( $*p < 0.05$ ,  $**p < 0.01$ ).

secretion. Medical Cannabis has been classically divided into three phenotypic chemovar groups according to its content of THC and CBD: Type I which is THC-predominant, Type II in which the two are balanced and Type III which is CBD-predominant<sup>37,38</sup>. Recently, new Cannabis chemovars are being developed, which comprise high amounts of CBG and are now known as Type IV<sup>36,38</sup>. Importantly, to date, high-CBG chemovars are not commercially available and patients are prescribed medical Cannabis based on the THC:CBD

ratio. In this work, we used for the first time a non-psychoactive Type IV chemovar and proved its supremacy over the highly used psychoactive Type I.

Extensive research over the past years showed that each regulatory myeloid subpopulation is influenced by different cytokines and chemokines<sup>39</sup>. Moreover, each MDSC subpopulation possesses a different degree of immunosuppressive capabilities<sup>40</sup>. Studies show that although PMN-MDSCs are more abundant in the TME, MO-MDSCs proffer a stronger immunosuppressive phenotype than PMN-MDSCs<sup>40</sup>. Moreover, a higher proportion of MO-MDSCs was previously found in peripheral blood from melanoma patients<sup>41</sup>, emphasizing the importance of targeting the MO-MDSC subpopulation. The successful targeting of MO-MDSC subpopulation and TAMs underlies CBG as a specific therapeutic tool for cancer patients with elevated circulating regulatory myeloid cells.

CBG-treated mice had no significant changes in MDSC frequencies in the tumor. This is possibly due to the fact that at this stage of the tumor progression, the most abundant myeloid subpopulations are differentiated macrophages. We did find, however, reduced MO-MDSCs frequencies in the spleens of treated mice, indicating lower amounts of circulating MO-MDSCs, possibly because less cells are recruited from the bone-marrow and expanded.

Although the connection between the endocannabinoid system and the immune system is well established, only a few studies focused on investigating its involvement in TME modulation. Because of the immunoregulatory properties of cannabinoids, the endocannabinoid system was previously suggested to play a fundamental role in shaping the TME and influencing tumor progression<sup>42</sup>. One study has shown the endocannabinoid 2-arachidonoylglycerol (2-AG) exhibits direct antitumor effects but also promotes an immunosuppressive microenvironment by increasing the suppressive immune cell population of MDSCs<sup>43</sup>. Another study focused on the effect of CBD on cytokine secretion in triple-negative breast cancer<sup>44</sup>. These studies, together with our results, support the potential of cannabinoids in modulating the TME in a variety of cancers. Moreover, we bring support for the utility of minor cannabinoids such as CBG in therapeutic settings.

Medical Cannabis is already being prescribed to cancer patients, primarily as palliative care meant to alleviate pain, relieve nausea and stimulate appetite<sup>45</sup>. A recent clinical trial tested the effectivity of CBG for sleep issues using 25–50 mg daily and did not report any toxicity side effects for this amount<sup>46</sup>, which is above the dose of CBG used in our study. Moreover, the average use of medical Cannabis in extract form is 1 gr a day, which is approximately 14 mg/kg/d, far greater

than the dose used in this study. We have previously shown medical Cannabis treatment is generally safe for oncology patients<sup>47</sup>. However, there is a huge variety between different medical Cannabis chemovars in their phytocannabinoid composition. A study that focused on the effect of synthetic THC on T-cell activity found it suppressed anticancer immunity<sup>48</sup>. In another study by our group, we found Cannabis consumption was associated with worsening the success rate of blockade therapy<sup>49,50</sup>. It is possible that these patients received medical Cannabis chemovars that were THC-rich, with very little CBG, indicating the pressing need for precision medicine that uses the proper treatment. Our findings have immediate practical implications; current treatment protocols that are already in combination with medical Cannabis as palliative care can select the CBG-rich chemovars in combination with immune checkpoint blockade therapy, making it more effective, and providing patients with antitumor properties in addition to the palliative ones<sup>52,53</sup>.

## Acknowledgments

The authors would like to thank Cannasoul Analytics and especially Dr Rotem Perry Feigenbaum for the isolation of the phytocannabinoid compounds; Ohad Guberman for the extraction and sample preparation of the Cannabis extracts; the Flow cytometry unit at the Technion Life Sciences and Engineering Infrastructure Center for the help with data analyses; and Yonathan Nissan at the Pre-Clinical Research Authority for help with the animal care. Diagrams were created with Biorender.

## Author contributions

IW, HNK and DM, Conceptualization and design; IW, MS, AG, RR, YEM and LS, Acquisition of data; IW and HNK, Analysis and interpretation of data; IW and SP Figure preparation; IW, HNK, SP and DM Writing, review, and/or revision of the manuscript, HNK and DM, Study supervision.

## Disclosure statement

D.M. is an active member of the scientific advisory board and co-founder of Cannasoul Analytics.

The rest of the authors have declared that no conflict of interest exists.

## Funding

This study was not supported by external funding.

## Data and materials availability

All data analyzed during this study are included in this published article and its supplementary information files. The datasets generated during the current study are available from the corresponding authors on reasonable request.

## Consent for publication

All authors give their consent to publish this manuscript.

## References

- Galli F, Aguilera JV, Palermo B, Markovic SN, Nisticò P, Signore A. Relevance of immune cell and tumor microenvironment imaging in the new era of immunotherapy. *J Exp Clin Cancer Res.* 2020;39(1):1–21. doi:10.1186/s13046-020-01586-y.
- Tcyganov E, Mastio J, Chen E, Gabrilovich DI. Plasticity of myeloid-derived suppressor cells in cancer. *Curr Opin Immunol.* 2019;51:76–82. doi:10.1016/j.coi.2018.03.009.
- Monteran L, Ershaid N, Doron H, Zait Y, Scharff Y, Ben-Yosef S, Avivi C, Barshack I, Sonnenblick A, Erez N. Chemotherapy-induced complement signaling modulates immunosuppression and metastatic relapse in breast cancer. *Nat Commun.* 2022;13(1). doi:10.1038/s41467-022-33598-x.
- Condamine T, Gabrilovich DI. Molecular mechanisms regulating myeloid-derived suppressor cell differentiation and function. *Trends Immunol.* 2011;32(1):19–25. doi:10.1016/j.it.2010.10.002.
- Laoui D, Van Overmeire E, De Baetselier P, Van Ginderachter JA, Raes G. Functional relationship between tumor-associated macrophages and macrophage colony-stimulating factor as contributors to cancer progression. *Front Immunol.* 2014;5(October):1–15. doi:10.3389/fimmu.2014.00489.
- Greten TF. Does CSF1R Blockade turn into friendly fire? *Cancer Cell.* 2018;32(5):546–547. doi:10.1016/j.ccell.2017.10.012.
- Ma T, Renz BW, Ilmer M, Koch D, Yang Y, Werner J, Bazhin AV. Myeloid-derived suppressor cells in solid tumors. *Cells.* 2022;11(2):310–322. doi:10.3390/cells11020310.
- Li T, Li X, Zamani A, Wang W, Lee C-N, Li M, Luo G, Eiler E, Sun H, Ghosh S, et al. C-Rel is a myeloid checkpoint for cancer immunotherapy. *Nat Cancer.* 2020;1(5):507–517. doi:10.1038/s43018-020-0061-3.
- Geiger R, Rieckmann JC, Wolf T, Basso C, Feng Y, Fuhrer T, Kogadeeva M, Picotti P, Meissner F, Mann M, et al. L-Arginine modulates T cell metabolism and enhances survival and anti-tumor activity article L-Arginine modulates T cell metabolism and enhances survival and anti-tumor activity. *Cell.* 2016;167(3):829–842.e13. doi:10.1016/j.cell.2016.09.031.
- Fares CM, Van Allen EM, Drake CG, Allison JP, Hu-Lieskovan S. Mechanisms of Resistance to Immune Checkpoint Blockade: why Does Checkpoint Inhibitor Immunotherapy Not Work for All Patients? *Am Soc Clin Oncol Educ B.* 2022;39:147–164. doi:10.1200/EDBK\_240837.
- Ries CH, Hoves S, Cannarile MA, Rüttinger D. CSF-1/CSF-1R targeting agents in clinical development for cancer therapy. *Curr Opin Pharmacol.* 2015;23:45–51. doi:10.1016/j.coph.2015.05.008.
- Baram L, Peled E, Berman P, Yellin B, Besser E, Benami M, Louria-Hayon I, Lewitus GM, Meiri D. The heterogeneity and complexity of Cannabis extracts as antitumor agents. *Oncotarget.* 2019;10(41):4091–4106. doi:10.18632/oncotarget.26983.
- Hinz B, Ramer R. Cannabinoids as anticancer drugs: current status of preclinical research. *Br J Cancer.* 2022;127(1):1–13. doi:10.1038/s41416-022-01727-4.
- Di Marzo V, Piscitelli F. The endocannabinoid system and its modulation by phytocannabinoids. *Neurotherapeutics.* 2015;12(4):692–698. doi:10.1007/s13311-015-0374-6.
- Lowe H, Toyang N, Steele B, Bryant J, Ngwa W. The endocannabinoid system: a potential target for the treatment of various diseases. *Int J Mol Sci.* 2021;22(17):22. doi:10.3390/ijms22179472.
- Jacobson MR, Watts JJ, Boileau I, Tong J, Mizrahi R. A systematic review of phytocannabinoid exposure on the endocannabinoid system: implications for psychosis. *Eur Neuropsychopharmacol.* 2019;29(3):330–348. doi:10.1016/j.euroneuro.2018.12.014.
- Straiker A, Wilson S, Corey W, Dvorakova M, Bosquez T, Tracey J, Wilkowski C, Ho K, Wager-Miller J, Mackie K, et al. An evaluation of understudied phytocannabinoids and their effects in two neuronal models. *Molecules.* 2021;26(17):1–17. doi:10.3390/molecules26175352.
- Berman P, Sulimani L, Gelfand A, Amsalem K, Lewitus GM, Meiri D. Cannabinoidomics – an analytical approach to understand the effect of medical Cannabis treatment on the endocannabinoid metabolome. *Talanta.* 2020;219:121336. doi:10.1016/j.talanta.2020.121336.
- Chakravarti B, Ravi J, Ganju RK. Cannabinoids as therapeutic agents in cancer: current status and future implications. *Oncotarget.* 2014;5(15):5852–5872. doi:10.18632/oncotarget.2233.
- Zagzoog A, Mohamed KA, Kim HJJ, Kim ED, Frank CS, Black T, Jadhav PD, Holbrook LA, Laprairie RB. In vitro and in vivo pharmacological activity of minor cannabinoids isolated from Cannabis sativa. *Sci Rep.* 2020;10(1):1–13. doi:10.1038/s41598-020-77175-y.
- Elliott DM, Singh N, Nagarkatti M, Nagarkatti PS. Cannabidiol attenuates experimental autoimmune encephalomyelitis model of multiple sclerosis through induction of myeloid-derived suppressor cells. *Front Immunol.* 2018;9:1–12.
- Passarelli A, Mannavola F, Stucci LS, Tucci M, Silvestris F. Immune system and melanoma biology: a balance between immunosurveillance and immune escape. *Oncotarget.* 2017;8(62):106132–106142. doi:10.18632/oncotarget.22190.
- Berman P, Futoran K, Lewitus GM, Mukha D, Benami M, Shlomi T, Meiri D. A new ESI-LC/MS approach for comprehensive metabolic profiling of phytocannabinoids in Cannabis. *Sci Rep.* 2018;8(1):1–15. doi:10.1038/s41598-018-32651-4.
- Galve-Roperh I, Chiurchiù V, Díaz-Alonso J, Bari M, Guzmán M, Maccarrone M. Prog Lipid Res Cannabinoid receptor signaling in progenitor/stem cell proliferation and differentiation. *Prog Lipid Res.* 2013;52(4):633–650. doi:10.1016/j.plipres.2013.05.004.
- Bronte V, Brandau S, Chen SH, Colombo MP, Frey AB, Greten TF, Mandruzzato S, Murray PJ, Ochoa A, Ostrand-Rosenberg S, et al. Recommendations for myeloid-derived suppressor cell nomenclature and characterization standards. *Nat Commun.* 2016;7(1):1–10. doi:10.1038/ncomms12150.
- Clementi E, Cervia D, Di Renzo I, Moscheni C, Bassi MT, Campana L, Martelli C, Catalani E, Giovarelli M, Zecchini S, et al. Nitric oxide generated by tumor-associated macrophages is responsible for cancer resistance to cisplatin and correlated with syntaxin 4 and acid sphingomyelinase inhibition. *Front Immunol.* 2018;9(May). doi:10.3389/fimmu.2018.01186.
- Zhou Y, Yoshida S, Kubo Y, Yoshimura T, Kobayashi Y, Nakama T, Yamaguchi M, Ishikawa K, Oshima Y, Ishibashi T. Different distributions of M1 and M2 macrophages in a mouse model of laser-induced choroidal neovascularization. *Mol Med Rep.* 2017;15(6):3949–3956. doi:10.3892/mmr.2017.6491.
- Patrinely JR, Baker LX, Davis EJ, Song H, Ye F, Johnson DB. Outcomes after progression of disease with anti – PD-1/PD-L1 therapy for patients with advanced melanoma. *Cancer.* 2020;126(15):3448–3455. doi:10.1002/ncr.32984.
- Sokolosky JT, Dougan M, Ingram JR, Chi C, Ho M, Kauke MJ, Ploegh HL, Garcia KC. Durable antitumor responses to CD47 blockade require adaptive immune stimulation. *Proc Natl Acad Sci USA.* 2016;113(19). doi:10.1073/pnas.1604268113.
- Fejza A, Polano M, Camicia L, Poletto E, Carobolante G, Toffoli G, Mongiat M, Andreuzzi E. The efficacy of anti-PD-L1 treatment in melanoma is associated with the expression of the ECM molecule EMILIN2. *Int J Mol Sci.* 2021;22(14):7511–7515. doi:10.3390/ijms22147511.
- Kalbasi A, Ribas A. Tumor-intrinsic resistance to immune checkpoint blockade. *Nat Rev Immunol.* 2021;20(1):25–39. doi:10.1038/s41577-019-0218-4.
- Postow MA, Callahan MK, Wolchok JD. Immune checkpoint blockade in cancer therapy. *J Clin Oncol.* 2015;33(17):1974–1982. doi:10.1200/JCO.2014.59.4358.
- Qiu Y, Su M, Liu L, Tang Y, Pan Y, Sun J. Clinical application of cytokines in cancer immunotherapy. *Drug Des Devel Ther.* 2021;15:2269–2287. doi:10.2147/DDDT.S308578.
- Yagiz K, Rittling SR. Both cell-surface and secreted CSF-1 expressed by tumor cells metastatic to bone can contribute to osteoclast activation. *Exp Cell Res.* 2010;315(14):2442–2452. doi:10.1016/j.yexcr.2009.05.002.
- Ding J, Guo C, Hu P, Chen J, Liu Q, Wu X, Cao Y, Wu J. CSF1 is involved in breast cancer progression through inducing monocyte

- differentiation and homing. *Int J Oncol.* 2016;49(5):2064–2074. doi:10.3892/ijo.2016.3680.
36. Nachnani R, Raup-Konsavage WM, Vrana KE. The pharmacological case for Cannabigerol. *J Pharmacol Exp Ther.* 2021;376(2):204–212. doi:10.1124/jpet.120.000340.
  37. Lewis MA, Russo EB, Smith KM, Village W, Republic C, Lewis M. Pharmacological foundations of Cannabis chemovars authors. *Planta Med.* 2018;84(4):225–233. doi:10.1055/s-0043-122240.
  38. Procaccia S, Lewitus GM, Lipson Feder C, Shapira A, Berman P, Meiri D. Cannabis for medical use: versatile plant rather than a single drug. *Front Pharmacol.* 2022;13(April):1–14. doi:10.3389/fphar.2022.894960.
  39. Kumar V, Patel S, Tcyganov E, Gabrilovich DI. The nature of myeloid-derived suppressor cells in the tumor microenvironment. *Trends Immunol.* 2017;37(3):208–220. doi:10.1016/j.it.2016.01.004.
  40. Youn J-I, Gabrilovich DI. The biology of myeloid-derived suppressor cells: the blessing and the curse of morphological and functional heterogeneity. *Eur J Immunol.* 2012;40(11):2969–2975. doi:10.1002/eji.201040895.
  41. Solito S, Marigo I, Pinton L, Damuzzo V, Mandruzzato S, Bronte V. Myeloid-derived suppressor cell heterogeneity in human cancers. *Ann Ny Acad Sci.* 2014;1319(1):47–65. doi:10.1111/nyas.12469.
  42. Kienzl M, Kargl J, Schicho R. The immune endocannabinoid system of the tumor microenvironment. *Int J Mol Sci.* 2020;21(23):8929. doi:10.3390/ijms21238929.
  43. Qiu C, Yang L, Wang B, Cui L, Li C, Zhuo Y, Zhang L, Zhang S, Zhang Q, Wang X. The role of 2-arachidonoylglycerol in the regulation of the tumor-immune microenvironment in murine models of pancreatic cancer. *Biomed Pharmacother.* 2019;115(May):108952. doi:10.1016/j.biopha.2019.108952.
  44. Elbaz M, Nasser MW, Ravi J, Wani NA, Ahirwar DK, Zhao H, Oghumu S, Satoskar A, Shilo K, Carson WE, et al. Modulation of the tumor microenvironment and inhibition of EGF/EGFR pathway: novel anti-tumor mechanisms of Cannabidiol in breast cancer. *Mol Oncol.* 2015;9(4):906–919. doi:10.1016/j.molonc.2014.12.010.
  45. Davis MP. Cannabinoids for symptom management and cancer therapy: the evidence. *J Natl Compr Cancer Netw.* 2016;14(7):915–922. doi:10.6004/jnccn.2016.0094.
  46. Emerson C Swallowable Cannabigerol tablets for sleep quality in veterans [Internet]. 2022. Available from: <https://clinicaltrials.gov/ct2/show/NCT05088018>
  47. Aviram J, Lewitus GM, Vysotski Y, Amna MA, Ouryvaev A, Procaccia S, Cohen I, Leibovici A, Akria L, Goncharov D, et al. The effectiveness and safety of medical Cannabis for treating cancer related symptoms in oncology patients. *Front Pain Res.* 2022;3(May):1–14. doi:10.3389/fpain.2022.861037.
  48. Xiong X, Chen S, Shen J, You H, Yang H, Yan C, Fang Z, Zhang J, Cai X, Dong X, et al. Cannabis suppresses antitumor immunity by inhibiting JAK/STAT signaling in T cells through CNR2. *Signal Transduct Target Ther.* 2022;7(1). doi:10.1038/s41392-022-00918-y.
  49. Bar-Sela G, Cohen I, Campisi-Pinto S, Lewitus GM, Oz-Ari L, Jehassi A, Peer A, Turgeman I, Vernicova O, Berman P, et al. Cannabis consumption used by cancer patients during immunotherapy correlates with poor clinical outcome. *Cancers (Basel).* 2020;12(9):12. doi:10.3390/cancers12092447.
  50. Taha T, Meiri D, Talhamy S, Wollner M, Peer A, Bar-Sela G. Cannabis impacts tumor response rate to nivolumab in patients with advanced malignancies. *Oncologist.* 2019;24(4):549–554. doi:10.1634/theoncologist.2018-0383.
  51. Hegde VL, Nagarkatti M, Nagarkatti PS. Cannabinoid receptor activation leads to massive mobilization of myeloid-derived suppressor cells with potent immunosuppressive properties. *Eur J Immunol.* 2010;40(12):3358–3371. doi:10.1002/eji.201040667.
  52. Wang X, Zhang J, Hu B, Qian F. High expression of CSF-1R predicts poor prognosis and CSF-1R high tumor-associated macrophages inhibit anti-tumor immunity in colon adenocarcinoma. *Front Oncol.* 2022;12(April):1–13. doi:10.3389/fonc.2022.850767.
  53. Liu H, Zhang H, Shen Z, Lin C, Wang X, Qin J, Qin X, Xu J, Sun Y. Increased expression of CSF-1 Associates with poor prognosis of patients with gastric cancer undergoing gastrectomy. *Medicine (Baltimore).* 2016;95(9):1–7. doi:10.1097/MD.0000000000002675.